



# Geographic and seasonal distributions of CO transport pathways and their roles in determining CO centers in the upper troposphere

L. Huang<sup>1</sup>, R. Fu<sup>1</sup>, J. H. Jiang<sup>2</sup>, J. S. Wright<sup>1</sup>, and M. Luo<sup>2</sup>

<sup>1</sup>Jackson School of Geosciences, The University of Texas at Austin, Austin, TX, USA

<sup>2</sup>Jet Propulsion Laboratory, California Institute of Technology, Pasadena, CA, USA

Correspondence to: R. Fu (rongfu@jsg.utexas.edu)

Received: 19 October 2011 – Published in Atmos. Chem. Phys. Discuss.: 9 December 2011

Revised: 8 May 2012 – Accepted: 8 May 2012 – Published: 30 May 2012

**Abstract.** Past studies have identified a variety of pathways by which carbon monoxide (CO) may be transported from the surface to the tropical upper troposphere (UT); however, the relative roles that these transport pathways play in determining the distribution and seasonality of CO in the tropical UT remain unclear. We have developed a method to automate the identification of two pathways (“local convection” and “advection within the lower troposphere (LT) followed by convective vertical transport”) involved in CO transport from the surface to the UT. This method is based on the joint application of instantaneous along-track, co-located, A-Train satellite measurements. Using this method, we find that the locations and seasonality of the UT CO maxima in the tropics were strongly correlated with the frequency of local convective transport during 2007. We also find that the “local convection” pathway (convective transport that occurred within a fire region) typically transported significantly more CO to the UT than the “LT advection → convection” pathway (advection of CO within the LT from a fire region to a convective region prior to convective transport). To leading order, the seasonality of CO concentrations in the tropical UT reflected the seasonality of the “local convection” transport pathway during 2007. The UT CO maxima occurred over Central Africa during boreal spring and over South America during austral spring. Occurrence of the “local convection” transport pathway in these two regions also peaked during these seasons. During boreal winter and summer, surface CO emission and convection were located in opposite hemispheres, which limited the effectiveness of transport to the UT. During these seasons, CO transport from the surface to the UT typically occurred via the “LT advection → convection” pathway.

## 1 Introduction

Biomass burning and fossil fuel combustion have long been recognized as globally important sources of trace gases and aerosols, especially in the tropics. Carbon monoxide (CO) plays a particularly influential role in global atmospheric chemistry. CO is a byproduct of the incomplete combustion of carbon-based fuels, and can also be produced by the oxidation of methane and non-methane hydrocarbons (Jacob, 1999). CO is an ozone ( $O_3$ ) precursor (Daniel and Solomon, 1998) and serves as the primary sink of the hydroxyl radical ( $OH$ ) (Thompson, 1992). The lifetime of CO in the tropical troposphere is 1–2 months, which makes it a useful tracer for studying the mass transport of air originating in regions of biomass burning or fossil fuel combustion (Edwards et al., 2006).

Previous studies based on observations and/or modeling (Novelli et al., 1998, 2003; Edwards et al., 2006; Duncan et al., 2007a; Junhua Liu et al., 2010; Macdonald et al., 2011) have shown that CO seasonal and interannual variability in the troposphere is affected by many factors, which can primarily be divided into the categories of photochemistry and transport. These factors vary greatly among different geographic regions.

Edwards et al. (2006) used five years of CO data from MO-PITT to show that the interannual variation of tropospheric CO in the Southern Hemisphere (SH) correlates well with the El Niño-Southern Oscillation (ENSO) precipitation index. Duncan et al. (2007a) evaluated the global budget of CO from 1988 to 1997 using a chemical transport model and found that emissions were largely constant during this period, as increases in Asia were offset by decreases elsewhere.

Junhua Liu et al. (2010) used model simulations to interpret the spatial and temporal variations of CO in the lower troposphere (LT) and upper troposphere (UT), and suggested that prevailing subsidence during the peak fire season over South America (July–August) may trap CO near the surface until convection associated with the inter-tropical convergence zone (ITCZ) moves into the fire region during September and October. Macdonald et al. (2011) investigated the relative influences of trans-Pacific transport and emissions from North American forest fires on CO concentration at a high elevation site using 5 yr of in-situ data. They argued that although trans-Pacific transport plays a role during boreal winter and spring, biomass burning is the most important contributor to periods of elevated CO concentration during summer.

Transport of CO from the surface to the UT has also been studied extensively using data from field campaigns, satellites, and numerical modeling simulations. Thompson et al. (1996), Pickering et al. (1996), and Andreae et al. (2004) have shown that local deep convection over fire regions can transport large amounts of CO to the UT. This “local convection” pathway is especially strong when the convection occurs in the form of pyrocumulonimbus clouds. CO may also be transported from a fire region to a convective region within the LT and then transported to the UT by deep convection (Folkins et al., 1997; Andreae et al., 2001). This “LT advection → convection” pathway is consistent with observations that UT CO centers are often located above convective regions rather than fire regions. This pathway may be particularly relevant because fires typically occur during dry seasons when local deep convection is infrequent. The existence and local importance of each of the two convection-induced transport pathways have been clearly demonstrated by previous case studies (e.g., Pickering et al., 1996; Folkins et al., 1997; Andreae et al., 2001, 2004; Williams et al., 2002); however, the roles and relative importance of the two pathways in determining the geographic and seasonal distributions of CO in the tropical UT have not yet been comprehensively evaluated.

Schoeberl et al. (2006) used satellite observations to describe a semi-annual cycle of CO in the UT and lower stratosphere (LS) with peaks in boreal spring (March–May) and fall (September–November). They suggested that these seasonal peaks of CO were related to seasonal peaks in biomass burning in Asia, Africa, and South America. Liu et al. (2007) compared the geographic and seasonal distributions of tropical deep convection with those of CO and water vapor in the UT, and suggested that the elevated concentrations of CO in the UT observed during boreal spring and fall may have been caused by the spatiotemporal coincidence of biomass burning emissions and deep convective activity over Africa and South America during these seasons. These previous studies (Schoeberl et al., 2006; Liu et al., 2007; Junhua Liu et al., 2010) suggest that spatial overlap between surface emission and deep convective activity enhances CO transport from the surface to the UT.

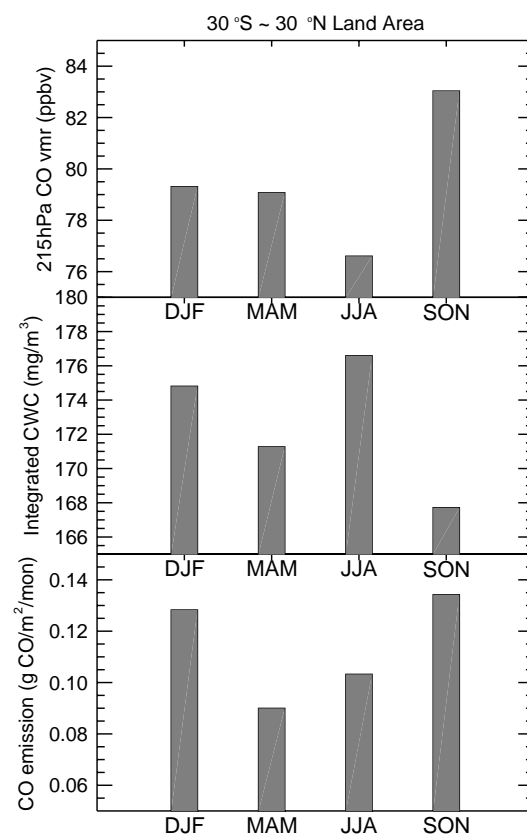


**Fig. 1.** Seasonal averages of MLS CO at 215 hPa (top), CloudSat cloud water content (CWC) vertically integrated above 6 km (middle), and GFED3 surface CO emission (bottom) over the tropical land area ( $30^{\circ}$  S– $30^{\circ}$  N) during December 2006–November 2007. The MLS CO values at 215 hPa have been scaled by 0.5 to compensate for the high bias.

Relationships between the seasonal cycle of CO concentration in the UT and the seasonal cycles of surface emission and convection are not straightforward. Emissions of CO at the surface peak during boreal fall and winter, and convective activity over the tropical land area between  $30^{\circ}$  S and  $30^{\circ}$  N peaks during boreal summer and winter (Fig. 1). Mean CO concentration in the UT peaks during boreal fall, when convective activity is at a minimum. Furthermore, the mean concentration of CO in the UT is higher during boreal spring than during summer, even though surface CO emission and convective activity are both higher during summer than during spring. The lack of correlations among peaks in mean CO concentration in the tropical UT and peaks in surface emission and convective activity highlights the potential importance of transport pathways.

Duncan et al. (2007b) studied troposphere-to-stratosphere (TST) transport of CO and evaluated the impacts of biomass burning pollution on the composition of the tropical tropopause layer (TTL) and lowermost stratosphere (LMS). They found that two TST pathways (slow ascent through

the TTL and quasi-horizontal exchange into the LMS) are of similar importance for the transport of biomass burning pollution. By contrast, our study focuses on the pathways that transport CO from the surface to the UT (215 hPa, below TTL) and how their seasonal variations influence the seasonal variation of UT CO over two important biomass burning regions. Junhua Liu et al. (2010) used GEOS-Chem model simulations to evaluate CO transport in the GEOS-4 and GEOS-5 assimilated meteorological fields and to identify causes of discrepancies between observations and simulations.

This study develops a method using co-located satellite measurements to automatically identify the two convection-induced CO transport pathways, and uses this method to study the relative importance of these two pathways to seasonal variations of CO in the tropical UT. Although CO concentration can be influenced by multiple transport pathways simultaneously, the two transport pathways defined here broadly represent long-range transport of CO from the surface to the UT, such as that associated with the ITCZ. Previous studies have used data from A-Train (L'Ecuyer and Jiang, 2010) satellites to study CO transport (e.g., Fu et al., 2006; Park et al., 2007; Barret et al., 2008; Halland et al., 2009; Junhua Liu et al., 2010; Jin et al., 2011). Here, we build upon these previous studies by presenting and applying an automated detection mechanism for the two CO transport pathways described above. This method streamlines the identification of CO transport pathways by intelligently combining instantaneous along-track observations of CO in the UT from the Aura Microwave Limb Sounder (MLS), observations of convective clouds from the CloudSat radar, and CO emissions derived from Moderate-resolution Imaging Spectroradiometer (MODIS) fire data, as described in Sects. 2 and 3. We apply the method to quantify the frequency of occurrence of each transport pathway with respect to the major centers of elevated CO in the tropical UT, as presented in Sect. 4. We are then able to evaluate the relative importance of the two pathways in determining the seasonality of UT CO over the selected domains, and to reconcile the mismatch between the seasonal cycle of UT CO and the seasonal cycles of surface CO emissions and convective activity, as shown in Sect. 5. The main conclusions of this work are summarized and discussed in Sect. 6.

## 2 Datasets

The seasonal distributions of CO concentration are described according to satellite observations taken by the Aura MLS for the upper troposphere and the Aura Tropospheric Emission Spectrometer (TES) for the lower troposphere. The location and relative strength of convective activity is estimated using satellite observations of cloud water content (CWC) taken by the CloudSat millimeter-wavelength cloud radar.

The Aura MLS detects CO in the UT/LS region by measuring thermal emission at 240 GHz with a limb-viewing geometry (Pumphrey et al., 2007; Livesey et al., 2008). The vertical resolution of the CO retrieval is approximately 4 km in the UT/LS, and the horizontal resolution is approximately 5 km across-track and 300–400 km along-track. We use Level 2 CO derived according to the MLS Version 2.2 (v2.2) retrieval algorithm and screen the data as recommended by Livesey et al. (2007). The valid CO data in the UT are provided at 215, 147, and 100 hPa. The MLS v2.2 CO data has a systematic factor of  $\sim 2$  high bias at 215 hPa, but the morphology is generally realistic (Livesey et al., 2008). We have also performed the pathway analysis using MLS Version 3.3 (v3.3) data. This version has eliminated the high positive bias at 215 hPa, but the ability of the retrieval to separate clouds and CO is considerably worse than in v2.2 (Livesey et al., 2011). Our results using v3.3 are similar to those using v2.2; accordingly, we only present results based on MLS v2.2 CO data in the following sections.

TES is an infrared Fourier transform spectrometer with high spectral resolution ( $0.1 \text{ cm}^{-1}$ ) and a wide spectral range ( $650\text{--}3050 \text{ cm}^{-1}$ ) (Beer et al., 2001; Beer, 2006). The footprint of each TES nadir observation is  $5 \times 8 \text{ km}$  (Beer, 2006). TES retrievals of CO are primarily sensitive to CO concentrations in the 700–200 hPa pressure range and have been found to be consistent with measurements made by the Measurements of Pollution in the Troposphere (MOPITT) satellite instrument (Luo et al., 2007b) and aircraft data (Luo et al., 2007a; Lopez et al., 2008). TES cannot reliably retrieve CO in the presence of clouds (Halland et al., 2009). We use V004 of the level 2 TES data (F05\_07) and screen the data according to the recommended guidelines (Osterman, 2009).

CloudSat carries the first space-borne 94-GHz cloud profiling radar (CPR) to measure vertical structures of cloud and precipitation (Stephens et al., 2002). Each CPR profile has a vertical resolution of  $\sim 500 \text{ m}$ , but the measurements are reported on an increment of  $\sim 240 \text{ m}$  with 125 vertical layers. The footprint for a single profile is approximately 1.3 km across-track by 1.7 km along-track, with along-track sampling spaced every 1.1 km (CloudSat Project, 2008). CWC represents the sum of cloud ice water content (IWC) and liquid water content (LWC) observed by CloudSat.

CO emission at the surface is obtained from the Global Fire Emission Database version 3 (GFED3) which has recently been released (van der Werf et al., 2010). This gridded data is provided at  $0.5 \times 0.5^\circ$  spatial resolution and monthly temporal resolution, and includes burned area and fire emissions. Emissions of fire-generated trace gases are derived by combining information on burned area with MODIS fire hot spots (Giglio et al., 2006, 2010), biogeochemical model estimates of fuel burned, and emission factors for each species. The approach used to derive daily CO emission from GFED3 monthly emissions is described by Mu et al. (2011).

### 3 Methodology

We select South America ( $24^{\circ}$  S– $12^{\circ}$  N,  $88$ – $32^{\circ}$  W) and Central Africa ( $20^{\circ}$  S– $20^{\circ}$  N,  $16^{\circ}$  W– $40^{\circ}$  E) as our domains. These are two of the most important tropical biomass burning regions and coincide with the locations of UT CO maxima in the tropics. CO has a relatively long lifetime in the UT. We evaluate the change of CO concentration in the UT by calculating the difference between instantaneous CO measurements at 215 hPa and monthly mean values interpolated from a  $4^{\circ}$  latitude  $\times$   $8^{\circ}$  longitude grid to the observational location and level. The threshold of CO increase is 20 ppbv, which coincides with the estimated precision of MLS CO at 215 hPa (Livesey et al., 2007). If the calculated change in UT CO exceeds 20 ppbv, it is defined as an increase of CO in the UT. We use vertically integrated CloudSat CWC above 6 km (iCWC\_6 km) to represent convective activity. The threshold for iCWC\_6 km is  $100 \text{ mg m}^{-3}$ , which is approximately the median value of all the iCWC\_6 km over the selected South America and Central Africa domains. If the observed iCWC\_6 km exceeds this value  $100 \text{ mg m}^{-3}$ , it is defined as deep convective activity. To justify the use of CloudSat CWC as an indicator of deep convection, we have compared it with the TRMM cloud feature database (Liu et al., 2008) and ISCCP D2 deep convective cloud amount data (Rossow and Schiffer, 1999). The spatial distributions of deep convection averaged over periods of 8 days or longer are nearly identical among these three datasets. Cirrus clouds that are not associated with convection typically have a much smaller CWC (Ström et al., 2003) than the convective anvils captured by our CWC threshold. Thus, CloudSat CWC is appropriate for identifying convective activity in this work. During the year 2007, Aura MLS and CloudSat measurements are separated by only 7–8 min in time, but their measurement tracks are separated by  $\sim 200$  km at low and middle latitudes (Savtchenko et al., 2008). Thus, MLS and CloudSat measurements are not exactly co-located for tropical clouds; however, because mesoscale convection is typically 100 km or more in size (Houze, 2004) and CO is a long-lived tracer, CloudSat observations are likely to be indicative of the convective conditions affecting UT CO along the MLS track. We co-locate CloudSat CWC with MLS CO measurements by averaging CWC in boxes of  $3^{\circ}$  along-track and  $1^{\circ}$  across-track centered on the MLS measurement locations (approximately matching the MLS footprints). To co-locate GFED3 daily CO emission with MLS observation, we first identify the  $0.5 \times 0.5^{\circ}$  grid box that contains the center of the MLS footprint, then check for surface CO emission within any of a  $5 \times 5$  set of grid boxes centered on the co-located grid box (i.e.,  $2.5 \times 2.5^{\circ}$  resolution).

The “local convection” pathway is identified when an increase of CO in the UT is detected simultaneously co-located with non-zero surface CO emission and deep convection. The “LT advection → convection” pathway is identified when an increase of CO in the UT is detected simultaneously

co-located with deep convection, but the co-located surface CO emission is zero. The effectiveness and validity of this method for identifying CO transport pathways is demonstrated in the following section, which describes a detailed case study.

### A case study

Figure 2a shows the spatial distributions of surface CO emission and MLS instantaneous, along-track measurements of CO concentration in the UT (215 hPa) on 12 January 2007. The strongest CO emission was located over northern Africa, while moderate CO emission occurred in northern South America and southern Brazil. The MLS detected high CO concentrations over the South American continent and southern Africa, south of the primary CO emission region in Africa (Fig. 2a). The southward displacement of the UT CO maximum relative to the surface emission region may suggest that CO was not directly transported to the UT by local convection.

To illustrate how CO transport pathways affect the UT CO concentration over Central Africa, we choose a vertical cross section along the MLS track which is parallel to the CloudSat track indicated by the blue line (Fig. 2a). This cross section is along the Aura satellite descending track from  $20^{\circ}$  N to  $20^{\circ}$  S; the starting and ending points are indicated by A and B, respectively (Fig. 2a and b). CO emission was occurring along this track from  $12^{\circ}$  N to nearly  $5^{\circ}$  S, while the increase of CO ( $>20$  ppbv) at 215 hPa was mainly located in the SH between the equator and  $14^{\circ}$  S. CO increases in the UT occurred with co-located deep convection and surface emission at latitudes between  $1^{\circ}$  S and  $5^{\circ}$  S, suggesting CO transport from the surface to the UT via the “local convection” pathway. CO increases between  $5$ – $8^{\circ}$  S and  $13$ – $14^{\circ}$  S were co-located only with deep convection, suggesting CO transport via the “LT advection → convection” pathway. The distinction between these two pathways is dependent upon the distribution of surface CO emission. Our automated detection method captures the occurrence of these pathways, as indicated by the red (“local convection”) and blue (“LT advection → convection”) markers (Fig. 2b).

As validation of our automated detection method, we integrate seven-member back trajectory ensembles from each 215 hPa observation along this MLS track. Each ensemble consists of one trajectory initialized from the center of the MLS footprint, four trajectories initialized at offsets of  $\pm 0.5^{\circ}$  in latitude and longitude, and two trajectories initialized at  $\pm 2$  K in potential temperature. The initial potential temperatures are calculated according to MLS retrievals of temperature at 215 hPa. The trajectories are calculated using a modified version of the Goddard Fast Trajectory model (Schoeberl and Sparling, 1995; Wright et al., 2011), driven by winds and heating rates from NASA’s Global Modeling and Assimilation Office (GMAO) Modern-Era Retrospective Analysis for Research and Applications (MERRA) reanalysis (Rienecker

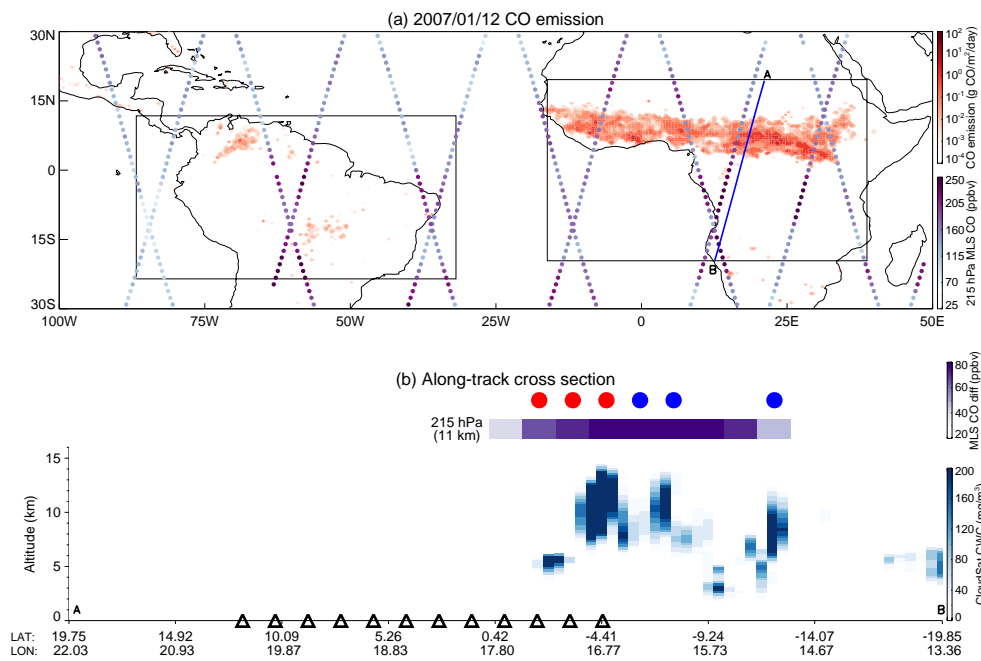


**Fig. 2.** (a) Spatial distributions of GFED3 surface CO emission and MLS instantaneous along-track measurements of CO concentration at 215 hPa on 12 January 2007. The solid blue line indicates the CloudSat track parallel to the MLS track selected for the case study discussed in Sect. 3; the starting and ending points are indicated by A and B, respectively. The two selected analysis domains are outlined by the black box: South America ( $24^{\circ}$  S– $12^{\circ}$  N,  $88^{\circ}$ – $32^{\circ}$  W) and Central Africa ( $20^{\circ}$  S– $20^{\circ}$  N,  $16^{\circ}$  W– $40^{\circ}$  E). (b) Vertical distributions of CloudSat CWC along the selected MLS track. Differences between observed CO volume mixing ratio and local monthly mean values at 215 hPa greater than 20 ppbv are shown in purple shading. The CloudSat CWC is from the original dataset, with the horizontal resolution reduced to  $\sim 0.5^{\circ}$ . The black triangles at the bottom indicate the presence of surface CO emissions along the cross section. The colored circles at the top indicate the CO transport pathways identified using the automated method, where red indicates “local convection” and blue indicates “LT advection  $\rightarrow$  convection”.

et al., 2011). The initial isentropic positions of the trajectories are calculated according to the corresponding Aura MLS retrievals of temperature at 215 hPa. Trajectories are initialized at the MLS observation (1 trajectory per ensemble), at  $\pm 0.5^{\circ}$  in latitude and longitude (4 trajectories per ensemble), and at  $\pm 2$  K in potential temperature (2 trajectories per ensemble), and were integrated backward in time for one day or until a convective source was identified.

We identify convective sources for each trajectory using two independent representations of convection: three-dimensional convective cloud fraction from the MERRA reanalysis (Rienecker et al., 2011) and cloud top pressure from the International Satellite Cloud Climatology Project (ISCCP) DX dataset (Rossow et al., 1996; Rossow and Schiffer, 1999). The MERRA cloud product is generated by the reanalysis model, and is provided as three-hour averages on a  $1.25 \times 1.25^{\circ}$  grid. Convective cloud top pressures are estimated using a linear interpolation in  $\ln(p)$ . We use 3-hourly ISCCP DX data from Meteosat-7 and Meteosat-8 for Central Africa, and from GOES-11 and GOES-12 for South America. We bilinearly interpolate cloud top pressures to the trajectory points from the gridded datasets, and identify convective intersections when cloud top pressures are (1) less

than trajectory pressures or (2) less than 350 hPa. This second threshold accounts for persistent low biases in infrared estimates of cloud top height (Sherwood et al., 2004) and is more in line with the representation of convection in the automated method (vertically-integrated CWC above 6 km). Convective intersections within 250 km of the trajectory initialization point are considered local.

The results of the trajectory simulations are in good agreement with the results of the automated detection mechanism (Fig. 3). The CO transport pathway identified by the automated method matches the pathway followed by the majority of trajectories in 24 out of 27 cases according to both representations of convection. For the other three cases, the automated method is only in disagreement with one of the two trajectory estimates (i.e., the two trajectory estimates also disagree with each other). At  $1.48^{\circ}$  S, the automated method identifies “local convection”; 71 % of the trajectories in this ensemble intersect with local ISCCP cloud tops, while none intersect with local MERRA cloud tops. Both ISCCP and MERRA indicate that the convective sources for some of these trajectories were located to the east of the MLS satellite track (in the same direction as the CloudSat track), but only ISCCP indicates that these sources were within 250 km

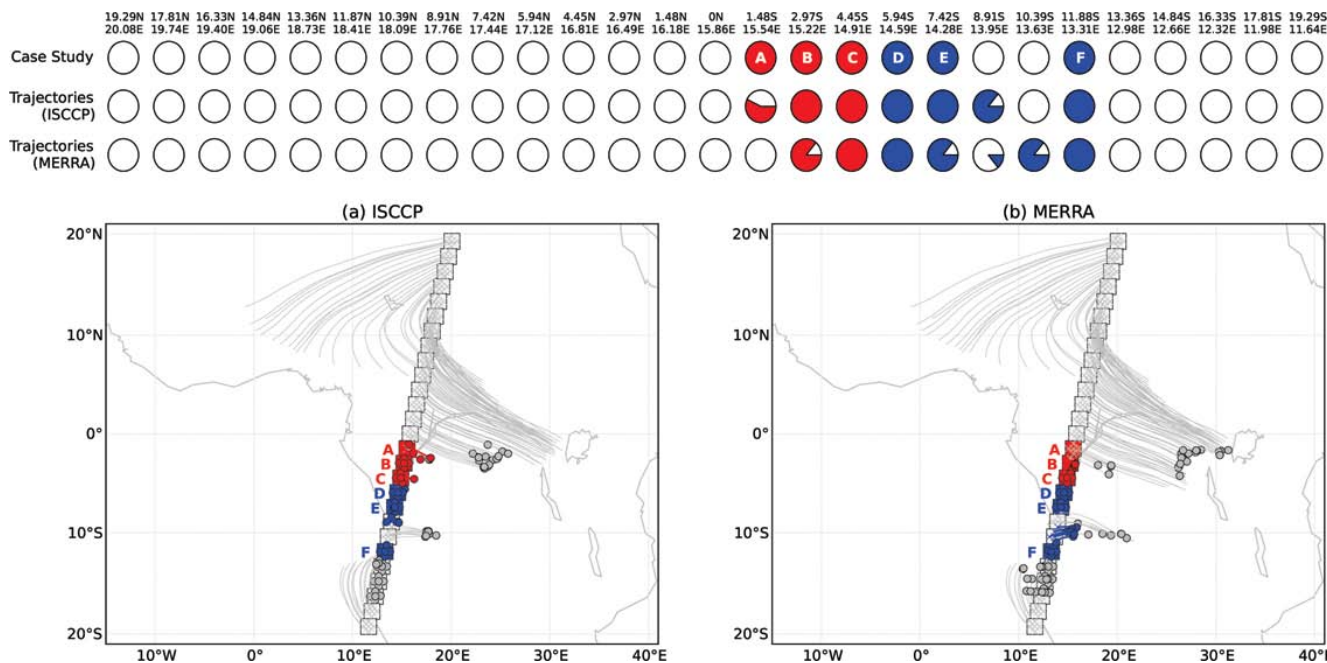


**Fig. 3.** Results of the trajectory analysis of CO transport for the case study shown in Fig. 2. **(a)** The evolution of trajectories (lines) and locations of convective sources (circles) according to ISCCP DX cloud tops. The pathway identified by the automated method is indicated by the color of the underlying square (red for “local convection”; blue for “LT advection → convection”), and the pathway identified by each trajectory is indicated by the color of the line and terminating circle (if any). **(b)** As in **(a)**, but according to MERRA cloud tops. The rows of circles along the top indicate the pathways identified by the automated method (first row), trajectories with ISCCP DX cloud tops (second row), and trajectories with MERRA cloud tops (third row) for individual MLS observations. Partially filled circles indicate fractions of trajectory ensembles. The labeled circles in the first row correspond to the similarly annotated locations in **(a)** and **(b)**.

of the trajectory starting points. The automated method does not identify convective transport at 8.91° S or 10.39° S. 86 % of the 8.91° S ensemble intersects with local ISCCP cloud tops and 14 % intersects with local MERRA cloud tops, while 86 % of the 10.39° S. Comparison of Figs. 2 and 3a–b suggests that these discrepancies are related to slight differences in the distributions of convection among these three datasets. For instance, it appears ISCCP indicates that the cluster of convection between the equator and ~8° S extends slightly further southward (Fig. 3a) than observed by CloudSat (Fig. 2) or simulated by MERRA (Fig. 3b). Meanwhile, MERRA simulates a cluster of convection to the east of the MLS track at 10.39° S (Fig. 3b) that ISCCP indicates is located further east (Fig. 3a) and CloudSat does not observe. Overall, our automated method performs well in comparison to the more computationally-expensive trajectory analysis. Discrepancies between the automated method and either trajectory ensemble are similar to discrepancies between the two trajectory ensembles, suggesting that uncertainties associated with the representation of convection are intrinsic to any study of convective transport in these regions. We have applied multiple representations of convection in different contexts (CloudSat CWC in the along-track automated method; CloudSat CWC, the TRMM cloud feature database and ISCCP D2 deep convective cloud amount in a coarse-

grain automated method; and ISCCP DX and MERRA in the trajectory analysis), and find that the results are qualitatively robust. We have also performed trajectory analyses for 11 other MLS tracks through Central Africa and South America on 12 January 2007, with similar results.

This case study shows that the two CO transport pathways can be successfully diagnosed through the joint use of Aura, CloudSat, and MODIS measurements at synoptic scales. Our detection criteria capture the relationships between surface CO emission, convective activity, and changes in UT CO that are associated with these transport pathways. We now apply this method to identify geographic and seasonal variations in the relative frequencies of occurrence of the two CO transport pathways over Central Africa and South America between December 2006 and November 2007.

#### 4 Seasonal distribution of CO transport pathways

Figures 4–7 show the seasonal mean geographic distributions of CO emission, convective activity, and CO in the LT (681 hPa) and UT (215 hPa) during the period December 2006–November 2007. The frequencies of occurrence of the different CO transport pathways are computed for each

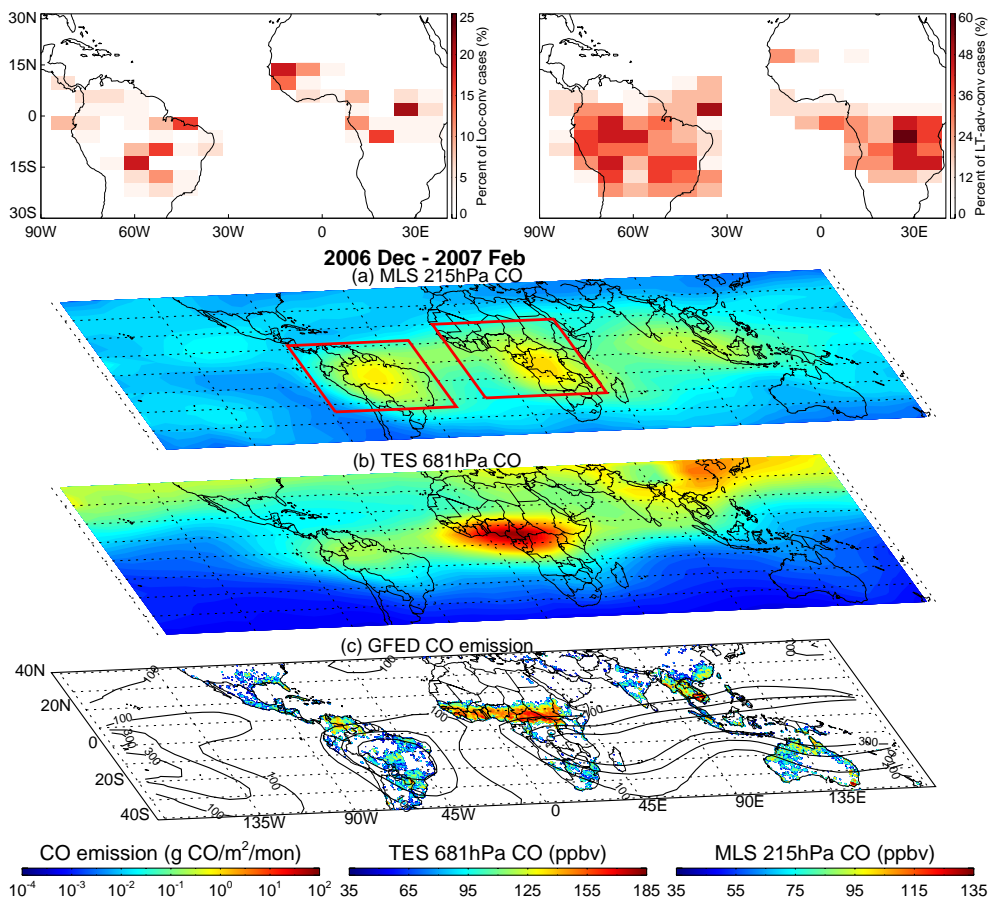


**Fig. 4.** Seasonal (December 2006–February 2007) mean distributions of (a) MLS CO in the upper troposphere (215 hPa, scaled by 0.5), (b) TES CO in the lower troposphere (681 hPa), and (c) GFED surface CO emission (color shading) and CloudSat CWC vertically integrated above 6 km (contours). The CWC contour interval is  $100 \text{ mg m}^{-3}$ . The two selected analysis domains are outlined in red: South America ( $24^{\circ} \text{ S}-12^{\circ} \text{ N}, 88^{\circ}-32^{\circ} \text{ W}$ ) and Central Africa ( $20^{\circ} \text{ S}-20^{\circ} \text{ N}, 16^{\circ} \text{ W}-40^{\circ} \text{ E}$ ). The two panels at the top show the spatial distributions of the relative frequency (percentage) of each transport pathway for each  $8 \times 4^{\circ}$  grid box in the two analysis domains: “local convection” (left), “LT advection → convection” (right).

domain. The boundaries of the two domains are denoted by red boxes in each figure.

During boreal winter, the strongest emission of fire-generated CO occurred in the savanna region of northern Africa (Fig. 4c). Deep convective activity was most pronounced over southern Africa, South America, and Indonesia, away from the strongest fire regions. In the LT (Fig. 4b), high CO concentrations were mainly located over the Gulf of Guinea and Central Africa, to the south of the primary CO emission region at the surface. The center of elevated CO in the UT over Central Africa was co-located with convective activity, also to the south of the primary CO emission region (Fig. 4a). Over South America, the CO maximum in the UT was located over the Amazon, to the southeast of the largest surface emissions. The displacement of CO maxima in the UT relative to surface emission regions and the co-location of these maxima with convective activity suggest that CO was advected southward within the LT from the emission regions

to the convective regions, then transported by deep convection to the UT.

The topmost panels of Fig. 4 show the spatial distributions of the relative frequency of each transport pathway in the two domains. The relative frequency is calculated as the percentage of each transport pathway normalized by the total number of CO increase cases within each  $4^{\circ}$  latitude  $\times 8^{\circ}$  longitude grid box. Burning was strongest between the equator and  $10^{\circ} \text{ N}$  in Africa; CO increases in the UT over northern Africa ( $0-15^{\circ} \text{ N}$ ) were primarily attributable to the “local convection” pathway. The “LT advection → convection” pathway was dominant in southern tropical Africa ( $8-20^{\circ} \text{ S}$ ), suggesting that CO from the primary burning regions north of the equator experienced southward cross-equatorial advection to the convective region, followed by deep convective transport to the UT. Over South America, the “LT advection → convection” pathway occurred over a large area within the analysis domain, while the “local convection” pathway

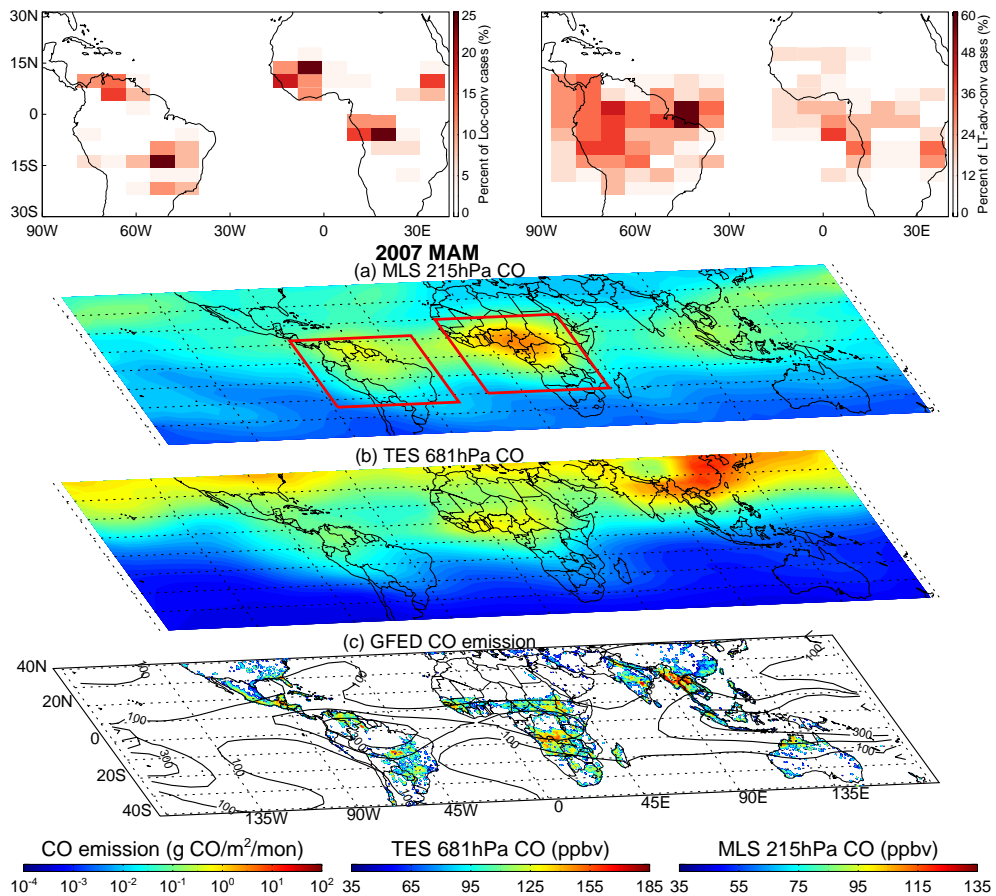


**Fig. 5.** As in Fig. 4, but for March–May 2007.

was mainly confined to the northwestern and southeastern corners. These results suggest that “LT advection → convection” was the dominant pathway for transporting CO to the UT over South America between December 2006 and February 2007.

During boreal spring (Fig. 5), CO emission was the strongest in Southeast (SE) Asia, and was relatively weak in Central Africa, Central America and northern South America (Fig. 5c). Deep convection was prevalent over equatorial Africa, South America, Central America and tropical Asia, all regions where CO emission occurred. In the LT over West Africa and SE Asia (Fig. 5b), high CO centers were collocated with surface emission, suggesting that CO was transported directly from the boundary layer to the LT. The largest CO concentrations in the UT were located over the Gulf of Guinea and Central Africa (Fig. 5a). This center of high UT CO had a greater geographic overlap with both high CO in the LT and areas of strong convection relative to that observed during the winter season (Fig. 4). Furthermore, greater overlap between convective activity and the fire source regions during boreal spring increased the occurrence and spatial coverage of the “local convection” pathway over the tropical southern African continent ( $20^{\circ}$  S– $2^{\circ}$  N) relative

to boreal winter, as shown in the top left panel. Over South America, UT CO concentrations were lower during boreal spring than during boreal winter (austral summer). This coincides with a reduction in the occurrences of both convective pathways. The reduction in the occurrence of the “LT advection → convection” pathway is more pronounced than that of the “local convection” pathway.

During boreal summer (Fig. 6), UT CO concentrations were highest over SE Asia, with a broad center of high CO extending from India in the West across southern China to the western Pacific Ocean in the East (Fig. 6a). CO over SE Asia is largely attributable to fossil fuel emissions (Duncan et al., 2007a; Jiang et al., 2007), which are not represented in the GFED3 CO emission dataset. Given this limitation of the GFED3 data, we instead focus our analysis on South America and Africa, where emissions of fire-generated CO are strongest (Fig. 6c). Most deep convective activity in these regions during boreal summer occurred over Central America and northern tropical Africa.

A center of high CO is apparent in the LT over the strong surface emissions in southern Africa (Fig. 6b), but not in South America. The daytime boundary layer and aerosol plumes are generally deeper over Africa (3–4.5 km, Labonne

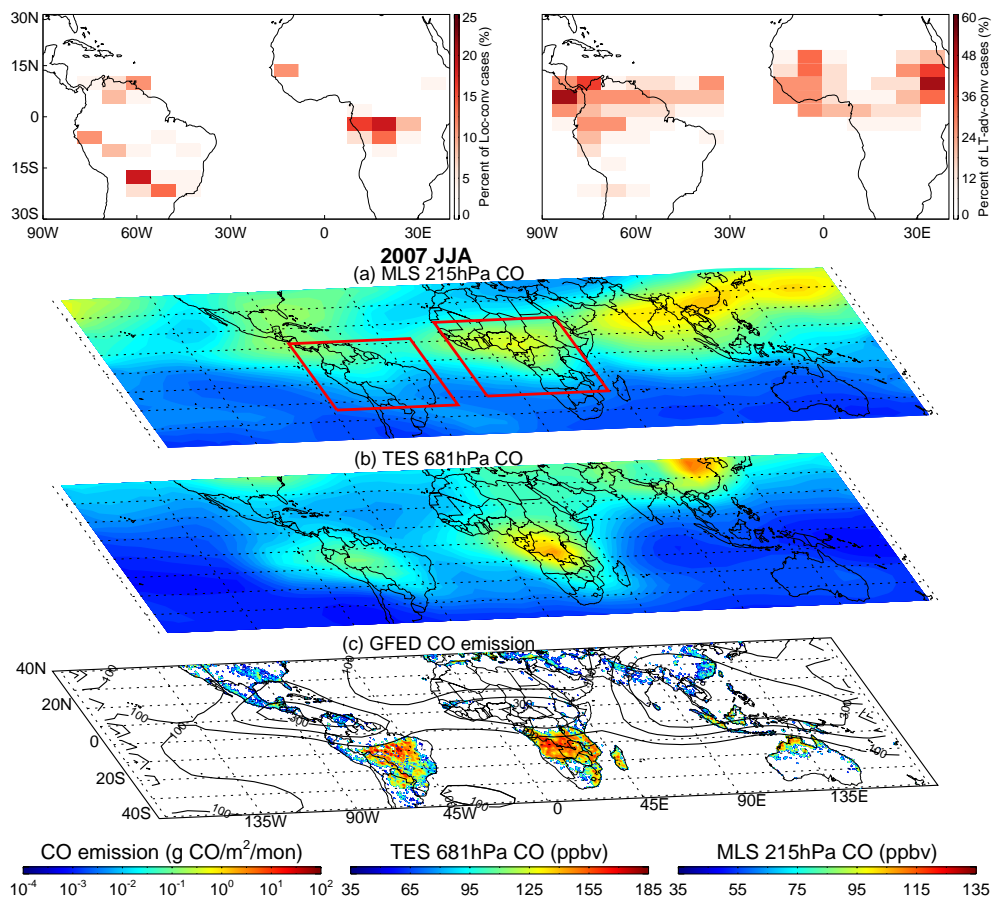


**Fig. 6.** As in Fig. 4, but for June–August 2007.

et al., 2007) than over South America (Martin et al., 1988; Fu et al., 1999). Smoke layers in the Amazon basin have been observed to reach 3 km in fire areas (Andreae et al., 2004), but the daytime boundary layer outside of active fire areas is generally shallower than 2 km (800 hPa) during this season. TES is sensitive to CO between 700 hPa and 200 hPa (Lopez et al., 2008). Because the boundary layer is deeper over Africa than over South America, high CO concentrations emitted over Central Africa are therefore more likely to be detected by TES. Extensive cloudiness over South America may also play a role by reducing the TES sampling rate.

High concentrations of CO in the LT and UT over equatorial western Africa suggest that CO originating in fires over southern Africa was transported by LT advection to West Africa, then lifted to the UT by convection associated with the African monsoon circulation. The “local convection” pathway was only prevalent in equatorial southern Africa ( $2\text{--}10^\circ \text{S}$ ). The locations of strongest CO emissions and deep convective activity are in opposite hemispheres relative to boreal winter (Fig. 4). This change causes a similar reversal in the preferred hemispheric locations of the “local convection” and “LT advection → convection” pathways. Over South America, the “local convection” pathway was preva-

lent over the southeastern part of the continent ( $16\text{--}24^\circ \text{S}$ ), while the “LT advection → convection” pathway was prevalent over northern South America ( $2^\circ \text{S}\text{--}12^\circ \text{N}$ , top panel of Fig. 6). The lack of a strong center of high CO in the UT over South America may be due to the relative weakness of convective activity, as shown in the bottom panel of Fig. 6.

During boreal fall (Fig. 7), the strongest surface CO emissions occurred in South America and southern Africa, with moderate CO emissions in northern Australia (Fig. 7c). Deep convective activity was centered over northern South America, Central Africa, and SE Asia. The largest CO concentrations in both the LT (Fig. 7b) and UT (Fig. 7a) were located over South America, suggesting that vertical transport of CO was locally strong. Indeed, the “local convection” pathway was dominant over much of South America during this season ( $4\text{--}24^\circ \text{S}$ , top panel of Fig. 7). A secondary center of high UT CO was observed over Central Africa. The “local convection” pathway was not as prevalent over Central Africa as over South America. In contrast to South America and Central Africa, CO remained low in the LT and UT over northern Australia despite strong surface emission. CO emissions appear to have been largely confined to the boundary layer in this region.

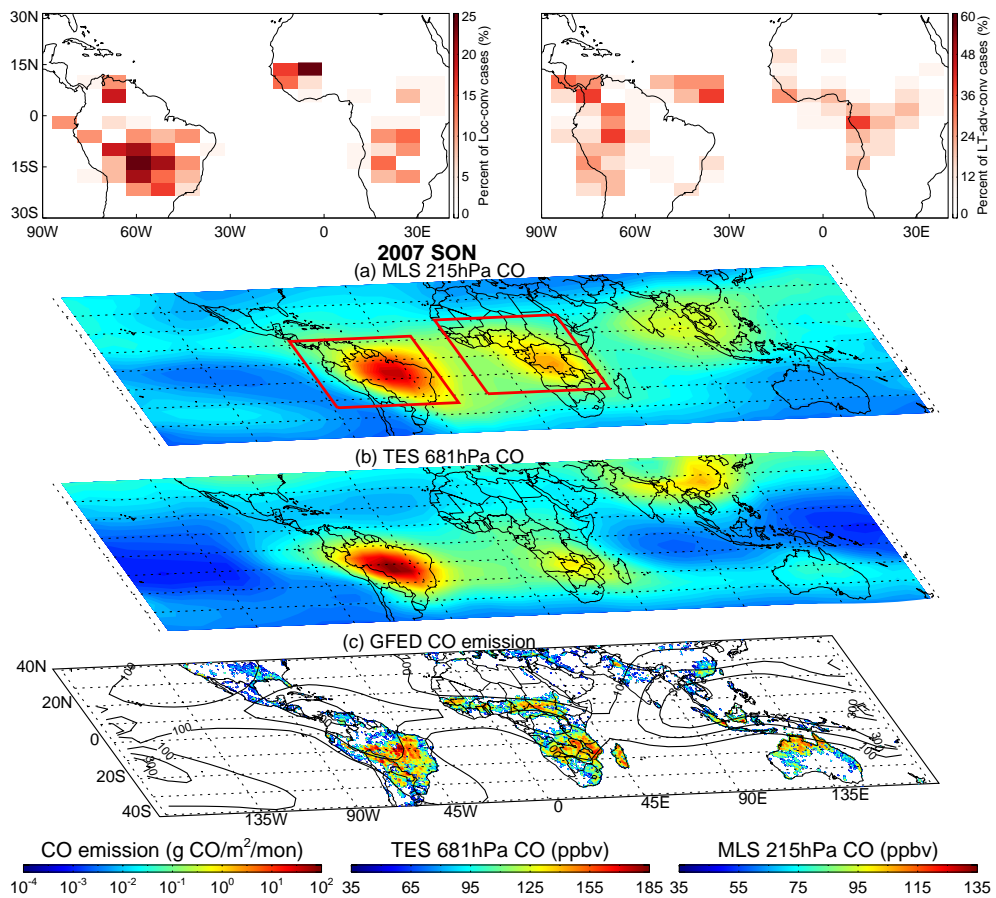


**Fig. 7.** As in Fig. 4, but for September–November 2007.

## 5 Discussion

The lifetime of CO in the troposphere is largely determined by the concentration of OH, its main sink (Levy II, 1971; Thompson, 1992). The levels of tropospheric hydroxyl radicals are strongly correlated with solar ultraviolet radiation (Rohrer and Berresheim, 2006) and have different seasonal cycles at various latitudes. The lifetime of CO in the troposphere is longer during local winter than during local summer, especially in the middle and higher latitudes (Duncan et al., 2007a). Because this work focuses on the tropical ( $20^{\circ}$  S– $20^{\circ}$  N) UT (215 hPa), seasonal changes in CO lifetime are therefore much less than those in the mid-latitudes.

Biomass burning represents the largest source of CO in the tropics during burning seasons, especially in the SH; during other seasons, oxidation of CH<sub>4</sub> and biogenic non-methane hydrocarbons (NMHC) may be more important (e.g., Logan et al., 1981; Holloway et al., 2000; Duncan et al., 2007a; Junhua Liu et al., 2010). The seasonal variations of CO production from biogenic sources and CH<sub>4</sub> oxidation at the surface and in the LT are also relatively small compared to the seasonal variations of biomass burning in the SH (Duncan et al., 2007a; Junhua Liu et al., 2010). In the UT, Junhua Liu

et al. (2010) used model simulations to show that seasonal changes in the biogenic source (from isoprene) do play an important role in the seasonality of UT CO over South America; however, biomass burning is the largest source of CO to the UT in burning regions during the biomass burning seasons (November–February in the NH, June–October in the SH). Therefore, the seasonal variations of CO in the tropical UT are likely to be largely determined by the convective transport of CO generated by biomass burning.

Figures 4–7 suggest that the seasonality of tropical mean UT CO concentration ( $25^{\circ}$  S– $25^{\circ}$  N) is controlled to leading order by seasonal changes in the centers of high UT CO over Central Africa and South America. Seasonal changes in the pathways that transport CO from the surface to the UT over these two regions therefore appear to play key roles in determining the seasonal cycle of UT CO in the tropics.

During our analysis period, CO emission over Central Africa peaked during boreal winter, while convective activity was nearly constant throughout the year (Fig. 8a, bottom two panels). Meanwhile, CO concentrations in the UT peaked during boreal spring and fall (Fig. 8a, top). The seasonal cycle of average CO increase reflects a combination of the two pathways; however, the “local convection” pathway

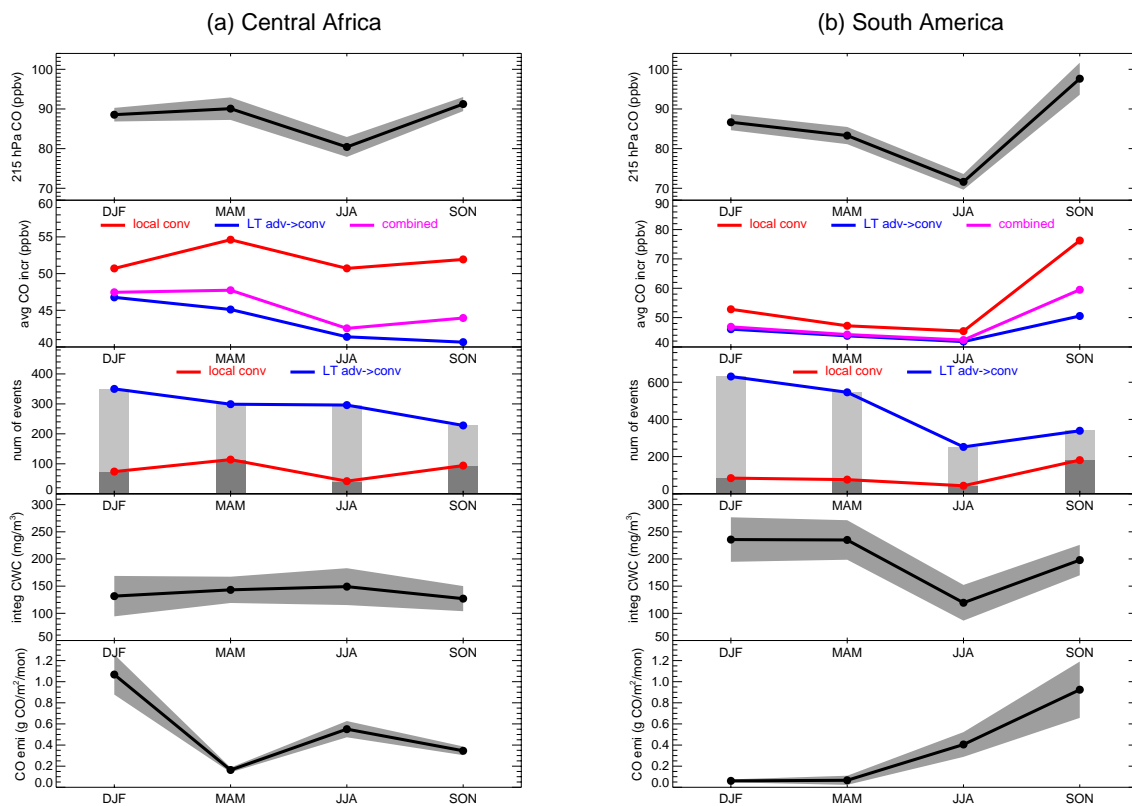


**Fig. 8.** Seasonal variation of: (top panel) MLS CO at 215 hPa (scaled by 0.5); (second panel from top) average CO increase associated with the “local convection” pathway (red line), with the “LT advection → convection” pathway (blue line) and with the combination of both pathways (purple line); (third panel from top) number of “local convection” pathway events (dark grey, red line) and number of “LT advection → convection” pathway events (light grey, blue line); (fourth panel from top) CloudSat vertically-integrated CWC above 6 km; and (bottom panel) GFED3 surface CO emission for (a) Central Africa ( $20^{\circ}$  S– $20^{\circ}$  N,  $16^{\circ}$  W– $40^{\circ}$  E) and (b) South America ( $24^{\circ}$  S– $12^{\circ}$  N,  $88$ – $32^{\circ}$  W) from December 2006–November 2007. The gray shaded areas around the 215 hPa CO, CWC and CO emission curves indicate  $\pm 2$  standard errors of the mean.

is the more influential of the two, and transports more CO per event during all seasons (Fig. 8a, second panel from top). Moreover, the seasonal variation of the number of “local convection” transport events (Fig. 8a, third panel from top) was similar to that of UT CO concentration. This result suggests that the seasonal prevalence of the “local convection” pathway plays a key role in the seasonal variation of UT CO over Central Africa. During boreal winter and summer, the primary fire regions and the convectively active regions were located in opposite hemispheres. Accordingly, the “local convection” transport pathway occurred infrequently, leading to lower concentrations of CO in the UT.

CO emission over South America peaked during austral spring, while deep convection peaked during austral summer and fall (Fig. 8b, bottom two panels). CO concentrations in the UT decreased monotonically from austral summer to winter, followed by a peak during austral spring. As with Central Africa, the seasonal variation of UT CO over South America was consistent with that of the number of “local convection” transport events, which again transports more

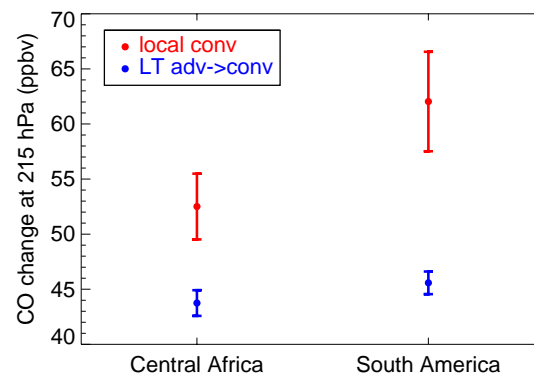


**Fig. 9.** Annual mean increases in CO concentrations at 215 hPa associated with the “local convection” (red) and “LT advection → convection” (blue) CO transport pathways. Error bars encompass  $\pm 2$  standard errors of the mean.

**Table 1.** Annual statistics of the two transport pathways. From left to right: first column indicates the domains; second and fourth columns indicate the total number of identified “local convection” and “LT advection → convection” transport events, respectively; third and fifth columns indicate the average CO increase associated with “local convection” and “LT advection → convection”, respectively; sixth column indicates the average CO increase associated with the combination of both pathways; seventh column indicates the difference between the average CO increase associated with “local convection” and the average CO increase associated with “LT advection → convection”. The numbers in the parentheses are  $\pm 2$  standard errors of the mean.

Domain	local convection		LT advection → convection		mean ΔCO combined (ppbv)	mean ΔCO difference (ppbv)
	num of events	mean ΔCO (ppbv)	num of events	mean ΔCO (ppbv)		
South America	382	62.0 ( $\pm 4.5$ )	1752	45.6 ( $\pm 1.0$ )	48.5 ( $\pm 1.2$ )	16.4
Central Africa	323	52.5 ( $\pm 3.0$ )	1179	43.7 ( $\pm 1.2$ )	45.6 ( $\pm 1.1$ )	8.8

CO per event than the other pathway during all seasons. Although the seasonal pattern of the number of “LT advection → convection” transport events is similar to that of UT CO, the number of “LT advection → convection” transport events peaks in austral summer rather than austral spring. The seasonality of UT CO over Central Africa and South America does not coincide with the seasonalities of surface CO emission or convective activity. Figure 8 suggests that it primarily coincides with the seasonality of CO transport by the “local convection” pathway. Furthermore, the seasonal pattern of the “local convection” pathway is effectively unchanged (not shown) when MERRA reanalysis data is used to eliminate cases with UT convergence (the presence of which might indicate advection from remote sources in the UT rather than local convective lofting), suggesting that the relationship between “local convection” and UT CO is not qualitatively influenced by advection of CO in the UT.

Figure 9 shows the annual average increase of CO concentrations at 215 hPa associated with the “local convection” and “LT advection → convection” transport pathways. Over Central Africa, the average increase of CO due to transport by “local convection” is approximately 5–13 ppbv (11–30 %) higher than that due to transport by “LT advection → convection”. Over South America, the increase of UT CO associated with “local convection” is about 11–22 ppbv (24–48 %) higher than that associated with “LT advection → convection”. These results suggest that the “local convection” pathway is more effective at transporting CO from surface to the UT than the “LT advection → convection” pathway, and provide a reasonable explanation for the similarity between the seasonal cycles of UT CO and the occurrence of the “local convection” pathway. The enhancement of CO increases over South America relative to those over Central Africa may be due to higher surface emissions and a more rapid advance of convection into the primary fire regions during the transition from dry season to wet season (Horel et al., 1989; Li and Fu, 2006). Table 1 presents the annual statistics of the two transport pathways in both analysis domains. Although the total number of “LT advection → convection” events is

much higher (3–5 times) than the total number of “local convection” events identified by our method, the average CO increase is significantly lower (as also shown in Fig. 9). These results indicate that the “local convection” pathway more efficiently transports CO from the surface to the UT, and they provide an explanation of the greater influence that this pathway exerts on the seasonal cycles of UT CO over Central Africa and South America.

## 6 Conclusions

We have presented a method that provides an automated identification of two pathways that transport CO from the surface to the UT through a joint use of several A-Train satellite measurements (including Aura MLS CO, Cloud-Sat CWC, and GFED CO emission derived from MODIS fire counts data). We have shown a case study that demonstrates the effectiveness and validity of this method based on comparison with the results of a back trajectory analysis. This method allows us to objectively identify CO transport pathways and provides a statistical description of the geographic and seasonal variations in these transport pathways. Seasonal UT CO distributions from December 2006 to November 2007 (Figs. 4–7) show that the primary centers of high UT CO were located over Central Africa during boreal spring and over South America during austral spring. In both of these regions, the seasonal cycle of UT CO coincided with the seasonal cycle of the frequency of the “local convection” pathway. This appears to be because the “local convection” pathway is significantly more effective at transporting CO to the UT than the “LT advection → convection” pathway. Convective activity and, to some extent, surface CO emissions were stronger during boreal winter and summer than during boreal spring and fall; however, CO emissions were generally located in the opposite hemisphere from convection during boreal winter and summer. Consequently, CO was typically transported via the “LT advection → convection” pathway over Central Africa during boreal winter and over South America during austral summer. The “LT advection

→ convection” pathway is less effective than the “local convection” pathway at transporting CO to the UT.

Our results also indicate geographic and seasonal variations in the distribution of convective CO transport pathways, with strong dependences on surface climate conditions and circulation patterns. We must therefore be cautious about generalizing these results, which are based on a limited time period. One source of uncertainty in our analysis is that we determine CO increase events as those individual measurements that exceed the background CO by 20 ppbv or more. This threshold is necessary due to the uncertainties in the MLS CO retrievals; however, this may omit many legitimate CO transport events for which the increase is less than 20 ppbv. This uncertainty could be avoided by directly evaluating daily changes of CO concentration. Such an evaluation is not realistic at present, but may be possible in the future with the advent of better measurements and improved retrieval algorithms.

The Atmospheric InfraRed Sounder (AIRS), which was launched aboard the Aqua satellite in 2002, also provides CO measurements (Aumann et al., 2003). AIRS takes measurements along a sun-synchronous orbit with a 1600 km wide swath, and can obtain high-density global CO retrievals even in the presence of substantial cloud cover (up to ~80%; Susskind et al., 2003). The AIRS CO products have improved substantially during recent years (Susskind et al., 2003; McMillan et al., 2011; Warner et al., 2007, 2010). For example, AIRS CO matches in-situ measurements from the NASA Intercontinental Chemical Transport Experiment (INTEX) to within 10 % for AIRS V4 (Warner et al., 2007) and to within 6–10 % for AIRS V5 (McMillan et al., 2011). The sensitivity of the AIRS CO retrieval peaks in the mid-troposphere, near 500 hPa (McMillan et al., 2011). In future work, we will further assess the climatological distributions of CO transport pathways over the tropical continents by applying the method that we have developed for this study to a longer period, which will enable further examination of UT CO variability at seasonal and interannual timescales. We will use all available CO products in this future work, including AIRS CO.

**Acknowledgements.** This work is supported by the NASA Aura Science Team program (NNX09AD85G), by the Jackson School of Geosciences at the University of Texas at Austin, and by the NASA Jet Propulsion Laboratory at the California Institute of Technology. We acknowledge the NASA CloudSat project for the CloudSat data. We also appreciate the comments from anonymous reviewers and editor Bryan Duncan that led to significant improvements in the manuscript.

Edited by: B. N. Duncan

## References

- Andreae, M. O., Artaxo, P., Fischer, H., Freitas, S. R., Gregoire, J. M., Hansel, A., Hoor P., Kormann, R., Krejci, R., Lange, L., Lelieveld, J., Lindner, W., Longo, K., Peters, W., de Reus, M., Scheeren, B., Silva-Dias, M. A. F., Strom, J., van Velthoven, P. F. J., and Williams, J.: Transport of biomass burning smoke to the upper troposphere by deep convection in the equatorial region, *Geophys. Res. Lett.*, 28, 951–954, doi:10.1029/2000GL012391, 2001.
- Andreae, M. O., Rosenfeld, D., Artaxo, P., Costa, A. A., Frank, G. P., Longo, K. M., and Silva-Dias, M. A. F.: Smoking rain clouds over the Amazon, *Science*, 303, 1337–1342, 2004.
- Aumann, H. H., Chahine, M. T., Gautier, C., Goldberg, M., Kalnay, E., McMillin, L., Revercomb, H., Rosenkranz, P. W., Smith, W. L., Staelin, D., Strow, L., and Susskind, J.: AIRS/AMSU/HSB on the aqua mission: design, science objectives, data products and processing systems, *IEEE T. Geosci. Remote.*, 41, 253–264, 2003.
- Barret, B., Ricaud, P., Mari, C., Attié, J.-L., Bouscerez, N., Josse, B., Le Flochmoën, E., Livesey, N. J., Massart, S., Peuch, V.-H., Piacentini, A., Sauvage, B., Thouret, V., and Cammas, J.-P.: Transport pathways of CO in the African upper troposphere during the monsoon season: a study based upon the assimilation of spaceborne observations, *Atmos. Chem. Phys.*, 8, 3231–3246, doi:10.5194/acp-8-3231-2008, 2008.
- Beer, R.: TES on the Aura Mission: Scientific Objectives, Measurements, and Analysis Overview, *IEEE T. Geosci. Remote*, 44, 1102–1105, 2006.
- Beer, R., Glavich, T. A., and Rider, D. M.: Tropospheric emission spectrometer for the Earth Observing System's Aura Satellite, *Appl. Optics*, 40, 2356–2367, 2001.
- CloudSat Project: CloudSat Standard Data Products Handbook, Cooperative Institutes for Research in the Atmosphere, Colorado State University, Fort Collins, CO, 2008.
- Daniel, J. S. and Solomon, S.: On the climate forcing of carbon monoxide, *J. Geophys. Res.*, 103, 13249–13260, doi:10.1029/98JD00822, 1998.
- Duncan, B. N., Logan, J. A., Bey, I., Megretskaya, I. A., Yantosca, R. M., Novelli, P. C., Jones, N. B., and Rinsland, C. P.: Global budget of CO, 1988–1997: Source estimates and validation with a global model, *J. Geophys. Res.-Atmos.*, 112, D22301, doi:10.1029/2007jd008459, 2007a.
- Duncan, B. N., Strahan, S. E., Yoshida, Y., Steenrod, S. D., and Livesey, N.: Model study of the cross-tropopause transport of biomass burning pollution, *Atmos. Chem. Phys.*, 7, 3713–3736, doi:10.5194/acp-7-3713-2007, 2007b.
- Edwards, D. P., Emmons, L. K., Gille, J. C., Chu, A., Attie, J. L., Giglio, L., Wood, S. W., Haywood, J., Deeter, M. N., Massie, S. T., Ziskin, D. C., and Drummond, J. R.: Satellite-observed pollution from Southern Hemisphere biomass burning, *J. Geophys. Res.*, 111, D14312, doi:10.1029/2005JD006655, 2006.
- Folkins, I., Chatfield, R., Baumgardner, D., and Proffitt, M.: Biomass burning and deep convection in southeastern Asia: Results from ASHOE/MAESA, *J. Geophys. Res.*, 102, 13291–13299, doi:10.1029/96JD03711, 1997.
- Fu, R., Zhu, B., and Dickinson, R. E.: How do atmosphere and land surface influence seasonal changes of convection in the tropical Amazon?, *J. Climate*, 12, 1306–1321, 1999.

- Fu, R., Hu, Y. L., Wright, J. S., Jiang, J. H., Dickinson, R. E., Chen, M. X., Filipiak, M., Read, W. G., Waters, J. W., and Wu, D. L.: Short circuit of water vapor and polluted air to the global stratosphere by convective transport over the Tibetan Plateau, *P. Natl. Acad. Sci. USA*, 103, 5664–5669, doi:10.1073/pnas.0601584103, 2006.
- Giglio, L., van der Werf, G. R., Randerson, J. T., Collatz, G. J., and Kasibhatla, P.: Global estimation of burned area using MODIS active fire observations, *Atmos. Chem. Phys.*, 6, 957–974, doi:10.5194/acp-6-957-2006, 2006.
- Giglio, L., Randerson, J. T., van der Werf, G. R., Kasibhatla, P. S., Collatz, G. J., Morton, D. C., and DeFries, R. S.: Assessing variability and long-term trends in burned area by merging multiple satellite fire products, *Biogeosciences*, 7, 1171–1186, doi:10.5194/bg-7-1171-2010, 2010.
- Hallard, J. J., Fuelberg, H. E., Pickering, K. E., and Luo, M.: Identifying convective transport of carbon monoxide by comparing remotely sensed observations from TES with cloud modeling simulations, *Atmos. Chem. Phys.*, 9, 4279–4294, doi:10.5194/acp-9-4279-2009, 2009.
- Holloway, T., Levy II, H., and Kasibhatla, P.: Global distribution of carbon monoxide, *J. Geophys. Res.*, 105, 12123–12147, doi:10.1029/1999JD901173, 2000.
- Horel, J. D., Hahmann, A. N., and Geisler, J. E.: An investigation of the annual cycle of convective activity over the tropical Americas, *J. Climate*, 2, 1388–1403, 1989.
- Houze, R. A.: Mesoscale convective systems, *Rev. Geophys.*, 42, RG4003, doi:10.1029/2004RG000150, 2004.
- Jacob, D. J.: Introduction to Atmospheric Chemistry, Princeton University Press, Princeton, New Jersey, USA, 1999.
- Jiang, J. H., Livesey, N. J., Su, H., Neary, L., McConnell, J. C., and Richards, N. A. D.: Connecting surface emissions, convective uplifting, and long-range transport of carbon monoxide in the upper-troposphere: New observations from the Aura Microwave Limb Sounder, *Geophys. Res. Lett.* 34, L18812, doi:10.1029/2007GL030638, 2007.
- Jin, J. J., Livesey, N. J., Jiang, J. H., Lupu, A., Kaminski, J. W., and McConnell, J. C.: Seasonal variation of trans-Pacific transport of carbon monoxide (CO) in the upper troposphere: MLS observations and GEOS-Chem and GEM-AQ simulations, *Atmos. Chem. Phys. Discuss.*, 11, 3219–3250, doi:10.5194/acpd-11-3219-2011, 2011.
- Junhua Liu, Logan, J. A., Jones, D. B. A., Livesey, N. J., Megretskaya, I., Carouge, C., and Nedelec, P.: Analysis of CO in the tropical troposphere using Aura satellite data and the GEOS-Chem model: insights into transport characteristics of the GEOS meteorological products, *Atmos. Chem. Phys.*, 10, 12207–12232, doi:10.5194/acp-10-12207-2010, 2010.
- Labonne, M., Bréon, F.-M., and Chevallier, F.: Injection height of biomass burning aerosols as seen from a spaceborne lidar, *Geophys. Res. Lett.*, 34, L11806, doi:10.1029/2007GL029311, 2007.
- L'Ecuyer, T. S. and Jiang, J. H.: Touring the atmosphere aboard the A-Train, *Phys. Today*, 63, 36–41, 2010.
- Levy II, H.: Normal Atmosphere: Large Radical and Formaldehyde Concentrations Predicted, *Science*, 173, 141–143, 1971.
- Li, W. H. and Fu, R.: Influence of Cold Air Intrusions on the Wet Season Onset over Amazonia, *J. Climate*, 19, 257–275, doi:10.1175/JCLI3614.1, 2006.
- Liu, C., Zipser, E. J., Cecil, D. J., Nesbitt, S. W., and Sherwood, S.: A cloud and precipitation feature database from 9 years of TRMM observations, *J. Appl. Meteorol. Clim.*, 47, 2712–2728, doi:10.1175/2008JAMC1890.1, 2008.
- Liu, C. T., Zipser, E., Garrett, T., Jiang, J. H., and Su, H.: How do the water vapor and carbon monoxide “tape recorders” start near the tropical tropopause?, *Geophys. Res. Lett.*, 34, L09804, doi:10.1029/2006GL029234, 2007.
- Livesey, N. J., Read, W. G., Lambert, A., Cofield, R. E., and Cuddy, D. T.: EOS MLS version 2.2 Level 2 data quality and description document, Jet Propulsion Laboratory, California Institute of Technology, Pasadena, CA, 2007.
- Livesey, N. J., Filipiak, M. J., Froidevaux, L., Read, W. G., Lambert, A., Santee, M. L., Jiang, J. H., Pumphrey, H. C., Waters, J. W., Cofield, R. E., Cuddy, D. T., Daffer, W. H., Drouin, B. J., Fuller, R. A., Jarnot, R. F., Jiang, Y. B., Knosp, B. W., Li, Q. B., Perun, V. S., Schwartz, M. J., Snyder, W. V., Stek, P. C., Thurstans, R. P., Wagner, P. A., Avery, M., Browell, E. V., Cammas, J. P., Christensen, L. E., Diskin, G. S., Gao, R. S., Jost, H. J., Loewenstein, M., Lopez, J. D., Nedelec, P., Osterman, G. B., Sachse, G. W., and Webster, C. R.: Validation of Aura Microwave Limb Sounder O<sub>3</sub> and CO observations in the upper troposphere and lower stratosphere, *J. Geophys. Res.*, 113, D15S02, doi:10.1029/2007JD008805, 2008.
- Livesey, N. J., Read, W. G., Froidevaux, L., Lambert, A., Manney, G. L.: EOS MLS version 3.3 Level 2 data quality and description document, Jet Propulsion Laboratory, California Institute of Technology, Pasadena, CA, 2011.
- Logan, J. A., Prather, M. J., Wofsy, S. C., and McElroy, M. B.: Tropospheric chemistry: A global perspective, *J. Geophys. Res.*, 86, 7210–7254, doi:10.1029/JC086iC08p07210, 1981.
- Luo, M., Rinsland, C., Fisher, B., Sachse, G., Diskin, G., Logan, J., Worden, H., Kulawik, S., Osterman, G., Eldering, A., Herman, R., and Shephard, M.: TES carbon monoxide validation with Dacom aircraft measurements during INTEX-B 2006, *J. Geophys. Res.*, 112, D24S48, doi:10.1029/2007JD008803, 2007a.
- Luo, M., Rinsland, C. P., Rodgers, C. D., Logan, J. A., Worden, H., Kulawik, S., Eldering, A., Goldman, A., Shephard, M. W., Gunson, M., and Lampel, M.: Comparison of carbon monoxide measurements by TES and MOPITT: Influence of a priori data and instrument characteristics on nadir atmospheric species retrievals, *J. Geophys. Res.*, 112, D09303, doi:10.1029/2006JD007663, 2007b.
- Lopez, J. P., Luo, M., Christensen, L. E., Loewenstein, M., Jost, H., Webster, C. R., and Osterman, G.: TES carbon monoxide validation during two AVE campaigns using the Argus and ALIAS instruments on NASA's WB-57F, *J. Geophys. Res.-Atmos.*, 113, D16S47, doi:10.1029/2007jd008811, 2008.
- Macdonald, A. M., Anlauf, K. G., Leitch, W. R., Chan, E., and Tarasick, D. W.: Interannual variability of ozone and carbon monoxide at the Whistler high elevation site: 2002–2006, *Atmos. Chem. Phys.*, 11, 11431–11446, doi:10.5194/acp-11-11431-2011, 2011.
- Martin, C. L., Fitzjarrald, D., Garstang, M., Oliveira, A. P., Greco, S., and Browell, E.: Structure and Growth of the Mixing Layer Over the Amazonian Rain Forest, *J. Geophys. Res.*, 93, 1361–1375, doi:10.1029/JD093iD02p01361, 1988.

- McMillan, W. W., Evans, K. D., Barnet, C. D., Maddy, E. S., Sachse, G. W., and Diskin, G. S.: Validating the AIRS Version 5 CO retrieval with DACOM in situ measurements during INTEX-A and -B, *IEEE T. Geosci. Remote.*, 49, 2802–2813, doi:10.1109/TGRS.2011.2106505, 2011.
- Mu, M., Randerson, J. T., van der Werf, G. R., Giglio, L., Kasibhatla, P., Morton, D., Collatz, G. J., DeFries, R. S., Hyer, E. J., Prins, E. M., Griffith, D. W. T., Wunch, D., Toon, G. C., Sherlock, V., and Wennberg, P. O.: Daily and 3-hourly variability in global fire emissions and consequences for atmospheric model predictions of carbon monoxide, *J. Geophys. Res.*, 116, D24303, doi:10.1029/2011JD016245, 2011.
- Novelli, P. C., Masarie, K. A., and Lang, P. M.: Distributions and recent changes of carbon monoxide in the lower troposphere, *J. Geophys. Res.*, 103, 19015–19033, 1998.
- Novelli, P. C., Masarie, K. A., Lang, P. M., Hall, B. D., Myers, R. C., and Elkins, J. W.: Reanalysis of tropospheric CO trends: effects of the 1997–1998 wildfires, *J. Geophys. Res.*, 108, 4464, doi:10.1029/2002JD003031, 2003.
- Osterman, G.: Earth Observing System (EOS) Tropospheric Emission Spectrometer (TES) Level 2 (L2) Data User's Guide (Up to & including Version 4 data), Jet Propulsion Laboratory, California Institute of Technology, Pasadena, CA, 2009.
- Park, M., Randel, W. J., Gettelman, A., Massie, S. T., and Jiang, J. H.: Transport above the Asian summer monsoon anticyclone inferred from Aura Microwave Limb Sounder tracers, *J. Geophys. Res.*, 112, D16309, doi:10.1029/2006JD008294, 2007.
- Pickering, K. E., Thompson, A. M., Wang, Y., Tao, W.-K., McNamara, D. P., Kirchhoff, V. W. J. H., Heikes, B. G., Sachse, G. W., Bradshaw, J. D., Gregory, G. L., and Blake, D. R.: Convective transport of biomass burning emissions over Brazil during TRACE A, *J. Geophys. Res.*, 101, 23993–24012, doi:10.1029/96JD00346, 1996.
- Pumphrey, H. C., Filipiak, M. J., Livesey, N. J., Schwartz, M. J., Boone, C., Walker, K. A., Bernath, P., Ricaud, P., Barret, B., Clerbaux, C., Jarnot, R. F., Manney, G. L., and Waters, J. W.: Validation of middle-atmosphere carbon monoxide retrievals from the Microwave Limb Sounder on Aura, *J. Geophys. Res.-Atmos.*, 112, D24S38, doi:10.1029/2007JD008723, 2007.
- Rienecker, M. M., Suarez, M. J., Gelaro, R., Todling, R., Bacmeister, J., Liu, E., Bosilovich, M. G., Schubert, S. D., Takacs, L., Kim, G.-K., Bloom, S., Chen, J., Collins, D., Conaty, A., da Silva, A., Gu, W., Joiner, J., Koster, R. D., Lucchesi, R., Molod, A., Owens, T., Pawson, S., Pigeon, P., Redder, C. R., Reichle, R., Robertson, F. R., Ruddick, A. G., Sienkiewicz, M., and Woollen, J.: MERRA: NASA's Modern-Era Retrospective Analysis for Research and Applications, *J. Climate*, 24, 3624–3648, doi:10.1175/JCLI-D-11-00015.1, 2011.
- Rohrer, F. and Berresheim, H.: Strong correlation between levels of tropospheric hydroxyl radicals and solar ultraviolet radiation, *Nature*, 442, 184–187, 2006.
- Rossow, W. B. and Schiffer, R. A.: Advances in Understanding Clouds from ISCCP, *B. Am. Meteorol. Soc.*, 80, 2261–2287, 1999.
- Rossow, W. B., Walker, A. W., Beuschel, D. E., and Roiter, M. D.: International Satellite Cloud Climatology Project (ISCCP): Documentation of new cloud Datasets, WMO/TD-No. 737, World Climate Research Programme (ICSU and WMO), Genf, 1996.
- Savtchenko, A., Kummerer, R., Smith, P., Gopalan, A., Kempler, S., and Leptoukh, G.: A-train data depot: bringing atmospheric measurements together, *IEEE T. Geosci. Remote.*, 46, 2788–2795, doi:10.1109/TGRS.2008.917600, 2008.
- Schoeberl, M. R. and Sparling, L.: Trajectory Modeling, in: Diagnostic Tools in Atmospheric Physics, edited by: Fiocco, G. and Visconti, G., Proceedings of the International School of Physics “Enrico Fermi”, 124, 289–306, 1995.
- Schoeberl, M. R., Duncan, B. N., Douglass, A. R., Waters, J., Livesey, N., Read, W., and Filipiak, M.: The carbon monoxide tape recorder, *Geophys. Res. Lett.*, 33, L12811, doi:10.1029/2006GL026178, 2006.
- Sherwood, S. C., Chae, J.-H., Minnis, P., and McGill, M.: Underestimation of deep convective cloud tops by thermal imagery, *Geophys. Res. Lett.*, 31, L11102, doi:10.1029/2004GL019699, 2004.
- Stephens, G. L., Vane, D. G., Boain, R. J., Mace, G. G., Sassen, K., Wang, Z., Illingworth, A. J., O'Connor, E. J., Rossow, W. B., Durden, S. L., Miller, S. D., Austin, R. T., Benedetti, A., Mitrescu, C., and the CloudSat Science Team: The CLOUDSAT mission and the A-TRAIN: A new dimension of space-based observations of clouds and precipitation, *B. Am. Meteorol. Soc.*, 83, 1771–1790, 2002.
- Ström, J., Seifert, M., Kärcher, B., Ovarlez, J., Minikin, A., Gayet, J.-F., Krejci, R., Petzold, A., Auriol, F., Haag, W., Busen, R., Schumann, U., and Hansson, H. C.: Cirrus cloud occurrence as function of ambient relative humidity: a comparison of observations obtained during the INCA experiment, *Atmos. Chem. Phys.*, 3, 1807–1816, doi:10.5194/acp-3-1807-2003, 2003.
- Susskind, J., Barnet, C. D., and Blaisdell, J. M.: Retrieval of atmospheric and surface parameters from AIRS/AMSU/HSB data in the presence of clouds, *IEEE T. Geosci. Remote.*, 41, 390–409, 2003.
- Thompson, A. M.: The Oxidizing Capacity of the Earth's Atmosphere: Probable Past and Future Changes, *Science*, 256, 1157–1165, 1992.
- Thompson, A. M., Pickering, K. E., McNamara, D. P., Schoeberl, M. R., Hudson, R. D., Kim, J. H., Browell, E. V., Kirchhoff, V. W. J. H., and Nganga, D.: Where did tropospheric ozone over southern Africa and the tropical Atlantic come from in October 1992? Insights from TOMS, GTE TRACE A, and SAFARI 1992, *J. Geophys. Res.*, 101, 24251–24278, doi:10.1029/96JD01463, 1996.
- van der Werf, G. R., Randerson, J. T., Giglio, L., Collatz, G. J., Mu, M., Kasibhatla, P. S., Morton, D. C., DeFries, R. S., Jin, Y., and van Leeuwen, T. T.: Global fire emissions and the contribution of deforestation, savanna, forest, agricultural, and peat fires (1997–2009), *Atmos. Chem. Phys.*, 10, 11707–11735, doi:10.5194/acp-10-11707-2010, 2010.
- Warner, J. X., Comer, M. M., Barnet, C. D., McMillan, W. W., Wolf, W., Maddy, E., and Sachse, G.: A comparison of satellite tropospheric carbon monoxide measurements from AIRS and MOPITT during INTEX-A, *J. Geophys. Res.*, 112, D12S17, doi:10.1029/2006JD007925, 2007.
- Warner, J. X., Wei, Z., Strow, L. L., Barnet, C. D., Sparling, L. C., Diskin, G., and Sachse, G.: Improved agreement of AIRS tropospheric carbon monoxide products with other EOS sensors using optimal estimation retrievals, *Atmos. Chem. Phys.*, 10, 9521–9533, doi:10.5194/acp-10-9521-2010, 2010.

Williams, J., Fischer, H., Wong, S., Crutzen, P. J., Scheele, M. P., and Lelieveld, J.: Near equatorial CO and O<sub>3</sub> profiles over the Indian Ocean during the winter monsoon: High O<sub>3</sub> levels in the middle troposphere and interhemispheric exchange, *J. Geophys. Res.*, 107, 8007, doi:10.1029/2001JD001126, 2002.

Wright, J. S., Fu, R., Fueglistaler, S., Liu, Y. S., and Zhang, Y.: The influence of summertime convection over Southeast Asia on water vapor in the tropical stratosphere, *J. Geophys. Res.*, 116, doi:10.1029/2010JD015416, 2011.